

APF-Based Control with Vortex Fields for Precise Robotic Manipulation in Grapevine Winter Pruning

Michela Andreotti, Miguel Fernandes, Angelo Bratta, Victor Barasuol, Claudio Semini

*Dynamic Legged Systems
Istituto Italiano di Tecnologia
Genova, Italy
name.surname@iit.it*

Abstract—In viticultural environments, trajectory planning for a robotic arm is particularly challenging due to the complex structure of grapevines. We propose a method for precise engagement of a robotic manipulator’s shears with grapevine canes during automated winter pruning. The approach utilizes artificial potential fields to guide the robot toward the target, while employing vortex fields to safely navigate the shears around obstacles detected from a 3D point cloud. Experimental results demonstrate that the method successfully guides the robot to the desired cane while avoiding collisions between the blades and the plant, enabling accurate and safe pruning operations in realistic vineyard conditions.

Index Terms—Precision Agriculture, Robotic Arm, Obstacle Avoidance Path Planning, Artificial Potential Fields, Vortex Fields

I. INTRODUCTION

Grapevine winter pruning represents a fundamental practice in viticulture, playing a decisive role in shaping plant growth and ensuring consistent fruit production. During winter pruning, portions of the growth from the previous season are carefully removed from dormant vines. The key purpose of this practice is to make precise cuts that retain specific canes and nodes, controlling the future growth of the plant and directly influencing the grape yield and quality [1].

This task can be divided into three challenging modules: grapevine 3D reconstruction, pruning point detection, and cut execution. In this paper, we will address the latter, while we refer to [2]–[4] for further information on the grapevine 3D reconstruction and how pruning points are selected.

The complex environment in which pruning is performed presents critical challenges. In particular, the robotic arm must navigate carefully around grapevine canes to determine the pruning path, avoiding damage to both the plant and the manipulator.

In this scenario, the robotic arm must combine reliable real-time performance with effective obstacle-avoidance capabilities, while being able to adapt its motion based on visual feedback. The Artificial Potential Field (APF) method is a well-established approach for trajectory planning, known for its good real-time performance and low computational effort [5], [6]. Unlike standard sampling-based methods [7], APF deterministic and continuous nature ensures consistent and

repeatable behaviour, essential for safe online pruning. APF-based strategies have been successfully applied in clustered environments, such as agriculture [8] and medical applications [9]. Nonetheless, the classical APF suffers from inherent drawbacks, most notably the proneness to local minima. To address this issue, the present work is formulated on the principle of vortex fields [10], [11] as an alternative avoidance strategy.

The main contribution of this paper is the application of APF-based techniques in the context of grapevine winter pruning, employing vortex fields for safe manoeuvring around obstacles. In particular, a real-time obstacle avoidance was implemented using camera-acquired inputs, and its performance was validated through preliminary hardware experiments (Fig. 1).

II. METHODS

A. Artificial Potential Fields

As already mentioned, APF is widely used for path planning [5], [6]. The main idea of the APF algorithm is to create virtual potential fields in Cartesian space, where the robot moves under the influence of an attractive potential toward



Fig. 1. Picture of the experimental setup showing the end-effector final approach and the simplified blade model. TCP is represented by the cross.

the goal and a repulsive potential away from obstacles. The linear attractive potential $U_a \in \mathbb{R}^3$ is defined as

$$U_a(\mathbf{q}) = \frac{1}{2} k_a \rho_g^2 \quad (1)$$

where $\mathbf{q} \in \mathbb{R}^{n_q}$ is the current joint position of the robot arm, $k_a \in \mathbb{R}^+$ is the attractive potential gain, and $\rho_g \in \mathbb{R}^3$ is the relative Cartesian distance between the Tool Centre Point (TCP) of the robot arm and the target position. In this work, the TCP is defined as the midpoint between the two blades of the custom shear end-effector, denoted by an ‘x’ in Fig. 1. Considering velocity control inputs, the gradient of (1) represents the attractive Cartesian velocity applied to the TCP [5], [9]. The function of the velocity can then be expressed as:

$$\nu_a = -\nabla U_a(\mathbf{q}) = k_a \rho_g \quad (2)$$

The angular velocity is processed in the same way as the linear velocity; it can be calculated by:

$$\omega_a = \zeta_a [\alpha \beta \gamma]^T \quad (3)$$

where the Euler angles $[\alpha \beta \gamma]^T \in \mathbb{R}^3$ are calculated from the quaternion representing the angular distance from the goal, and $\zeta_a \in \mathbb{R}^+$ is the coefficient of the attractive angular velocity. The construction of the repulsive potential field is similar to that of the attractive potential field. For every obstacle O_i , it can be defined as:

$$U_{r,i}(\mathbf{q}) = \begin{cases} \frac{k_{r,i}}{\gamma} \left(\frac{1}{\eta_i(\mathbf{q})} - \frac{1}{\eta_{0,i}} \right)^\gamma & \text{if } \eta_i(\mathbf{q}) \leq \eta_{0,i} \\ 0 & \text{if } \eta_i(\mathbf{q}) > \eta_{0,i} \end{cases} \quad (4)$$

where $\gamma = 2, 3, \dots$, $k_{r,i} \in \mathbb{R}^+$ is the repulsive gain, $\eta_i(\mathbf{q}) \in \mathbb{R}$ is the shortest distance to the obstacle and $\eta_{0,i} \in \mathbb{R}^+$ is the range of influence of the potential field. In this case, obstacles are derived from the point cloud obtained during the 3D reconstruction, as described in our previous work [4]. Each point in the point cloud is treated as the centre of a spherical object with radius r , resulting in a set of spherical obstacles to be avoided.

In the artificial potential field framework, any point on the robot can be influenced by the repulsive potential. The obstacle avoidance problem for manipulators is commonly formulated in terms of preventing collisions between the robot’s links, each of which can be represented as a line segment defined by two adjacent joints or points. Collision avoidance is then achieved by continuously controlling the link’s closest point to the obstacle [6]. The repulsive velocity of this point, referred to as the Point Subjected to the Potential (PSP), is given by:

$$\begin{aligned} \nu_{psp,i}(\mathbf{q}) &= -\nabla U_{r,i}(\mathbf{q}) \\ &= \begin{cases} \alpha(\mathbf{q}) \nabla \eta_i(\mathbf{q}) & \text{if } \eta_i(\mathbf{q}) \leq \eta_{0,i}, \\ 0 & \text{if } \eta_i(\mathbf{q}) > \eta_{0,i}. \end{cases} \end{aligned} \quad (5)$$

With $\alpha(\mathbf{q}) = \frac{k_{r,i}}{\eta_i^2(\mathbf{q})} \left(\frac{1}{\eta_i(\mathbf{q})} - \frac{1}{\eta_{0,i}} \right)^{\gamma-1}$.

The distance $\eta_i(\mathbf{q})$ is thus simply defined as the Cartesian distance between the PSP and the object’s centre, taking the radius into account.

In this work, considering the geometry of the blades, two PSPs are defined at each iteration by introducing artificial links. These links correspond to the outer distal halves of the left and right blades, as shown in Fig. 1. Their influence ranges are specifically tuned to prevent collisions between the blades and the plant, while avoiding any interference with the TCP located centrally between the two blades. The total potential $U_t(\mathbf{q})$ is obtained by superposition of the attractive and the aggregate repulsive potential, resulting in the velocity:

$$\nu_t(\mathbf{q}) = -\nabla U_t(\mathbf{q}) = \nu_a(\mathbf{q}) + \sum_{i=1} \nu_{r,i}(\mathbf{q}) \quad (6)$$

Where $\nu_{r,i}(\mathbf{q})$ denotes the repulsive velocity $\nu_{psp,i}(\mathbf{q})$ expressed with respect to the TCP, for each PSP.

B. Joint Velocities: Damped Least-Squares approach

In order to control the robot, velocities in Cartesian space need to be converted into joint space. The mapping relationship between the Cartesian space velocity and the joint speed of the APP can be expressed, using the Jacobian matrix $J \in \mathbb{R}^{6 \times n_q}$, as follows [5]:

$$\dot{\mathbf{q}} = J^{-1} \mathbf{V}_t(\mathbf{q}) \quad (7)$$

Here, $\mathbf{V}_t(\mathbf{q}) \in \mathbb{R}^6$ denotes the total velocity vector, defined as $\mathbf{V}_t(\mathbf{q}) = [\nu_t \ \omega_a]^T$, since there is no repulsive angular velocity.

A significant issue in Cartesian-space path planning is the occurrence of singularities, where the robot loses one or more degrees of freedom. To address this, the present work employs a Damped Least-Squares (DLS) approach with a dynamic damping factor [5], [12]. While this method may slightly reduce the accuracy of the TCP trajectory, it prevents singularities. The function of the damped least squares solution is defined as:

$$\dot{\mathbf{q}} = J^T (\lambda I + JJ^T)^{-1} \mathbf{V}_t(\mathbf{q}) \quad (8)$$

where $I \in \mathbb{R}^{6 \times 6}$ denotes the identity matrix and $\lambda \in \mathbb{R}$ is the dynamic damping factor, designed to be zero far from singularities and to increase near singular configurations, where joint velocities may become infeasible. Specifically, λ is adjusted based on the manipulability measure $\omega = \sqrt{\det(JJ^T)}$ with a threshold $\omega_t \in \mathbb{R}^+$: no damping is applied when $\omega > \omega_t$, and it progressively increases as ω decreases, reaching its maximum value $\lambda_0 \in \mathbb{R}^+$ at $\omega = 0$.

$$\lambda = \begin{cases} \lambda_0 \left(1 - \frac{\omega}{\omega_t} \right)^2 & \text{if } \omega < \omega_t \\ 0 & \text{if } \omega \geq \omega_t \end{cases} \quad (9)$$

C. Vortex Fields

The main drawback of artificial potential fields is the generation of local minima in the total field, which can cause the planning algorithm to get stuck. Vortex fields address this issue by guiding the robot to turn around obstacles [10].

Specifically, the direction of the repulsive velocity should be perpendicular to the radial vector between the obstacle and the point subjected to the potential, while the field intensity remains unchanged. A possible solution is given as follows:

$$\nu_{v,i}(\mathbf{q}) = \pm \begin{bmatrix} \frac{\partial U_{r,i}}{\partial y} \\ -\frac{\partial U_{r,i}}{\partial x} \\ 0 \end{bmatrix} \quad (10)$$

A critical aspect is the choice of the vortex rotation direction, since for articulated manipulators an inappropriate selection may prevent algorithm convergence and even cause the robot to collide with obstacles.

In the specific context of winter pruning, two scenarios must be distinguished: some canes represent obstacles to be avoided along the path to the goal, while others correspond to the pruning point, i.e., the goal itself. Consequently, the rotation rule is scenario-dependent. When navigating around an obstacle, the end-effector should rotate away from it, counter-clockwise if moving toward the TCP positive x direction, and clockwise otherwise. When approaching a pruning point, the end-effector should rotate toward the target, counter-clockwise if the PSP lies on the TCP positive x side, and clockwise otherwise.

III. RESULTS

To evaluate the proposed method, experiments were conducted using a Kinova Gen3 robotic arm equipped with custom end-effector shears (Fig. 1) and an Intel D405 camera. The velocity commands were transmitted through the joint trajectory controller of the *ros2_control* framework [13]. Information regarding the robot over time, including the Jacobian matrix and the TCP position, was obtained via the robotic manipulation platform *MoveIt 2* [14]. The point cloud is obtained with the 3D reconstruction approach introduced in [4].

The experiment was conducted with the robotic arm positioned in front of the grapevine plant, requiring the manipulator to reach a pruning point located diagonally with respect to the TCP. Upon examination of Fig. 2 and Fig. 3, it can be observed that the target point is successfully reached without the blades colliding with any obstacles.

In particular, Fig. 2 illustrates the trajectory of the TCP projected onto the $x-y$ plane. The grey line represents the path of the TCP, while the discrete ‘x’ markers indicate sampled positions at intervals of ≈ 0.70 seconds. For clarity, the simplified blade model from Fig. 1 is also included, with its distal links corresponding to those used in the repulsive force analysis. Additionally, the relevant portion of the cane involved in the motion is depicted by projecting the corresponding points of the point cloud onto the $x-y$ plane.

At the beginning of the motion, the TCP is driven solely by the attractive velocity (Fig. 3). As the TCP approaches the goal, this component gradually decreases, slowing down the motion. This effect is also evident from the increasingly dense distribution of the sampled TCP positions. Consequently, as the blades approach the cane, the repulsive velocity alters the trajectory of the arm. Specifically, the trajectory of the TCP is modified once the obstacles enter the range of influence

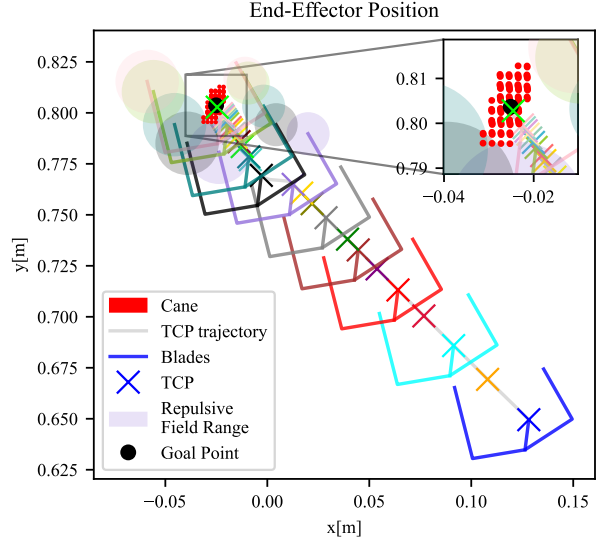


Fig. 2. TCP trajectory projected onto the $x-y$ plane with simplified blade model

of the repulsive potential field. This range is illustrated by circles centred at the PSPs of the blades. As a result of the choice of placing additional links on the distal outer portions of the blades and selecting a suitable influence radius, these circles cover the area effectively occupied by the blades while preserving a clearance from the cane, particularly along the outer edges, thereby ensuring collision avoidance. When the circles intersect the red points representing the cane, the obstacles enter the influence range of the repulsive field, and the resulting repulsive velocity is applied to the TCP to maintain a safe distance.

Indeed, by analysing the sampled TCP positions, it can be noted that the direction of the trajectory remains unaltered as long as the obstacles are outside the influence range (i.e., before the state shown in purple). In correspondence with the purple state, the obstacles enter this range (the circle is touching the obstacles), so the trajectory is deflected. As a consequence, in the following black and teal states, the blade (and the corresponding PSP) rotates around the obstacle due to the repulsive velocity (Fig. 3).

The rotation direction is correctly defined to guarantee a proper approach of the TCP to the pruning point. Finally, at the end of the motion, the obstacles are no longer within the range of influence of the repulsive force (green and pink states). As a result, the motion is successfully completed: the Tool Centre Point reaches the goal without any blade collisions, the final attractive velocity becomes null, and the approach is executed correctly (Fig. 1).

IV. CONCLUSION

This work demonstrates the successful application of APF-based path planning for a robotic manipulator performing

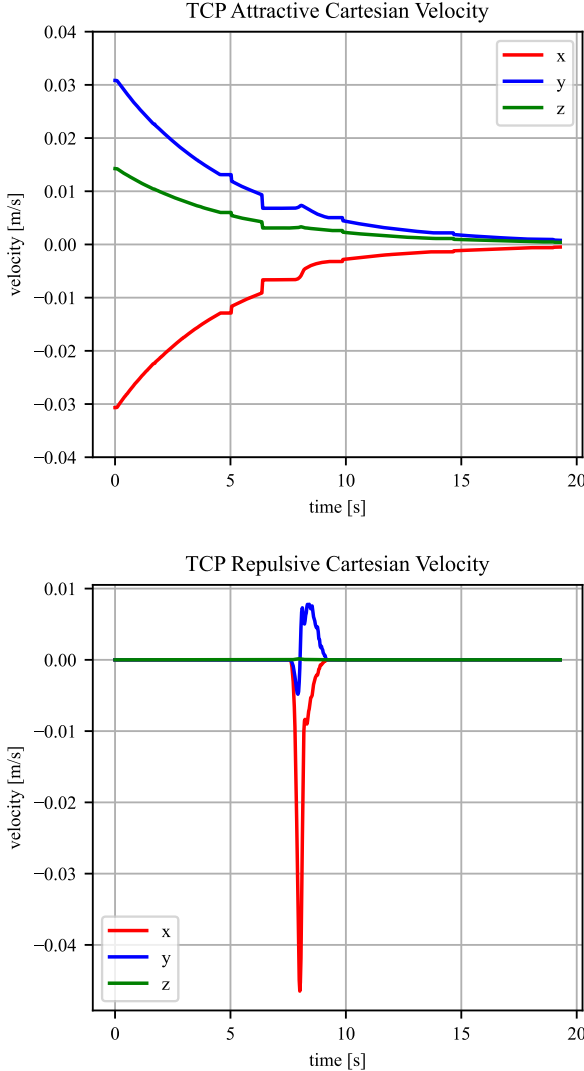


Fig. 3. Attractive and Repulsive Cartesian velocities of the Tool Centre Point over time

automated grapevine winter pruning. By integrating vortex fields for repulsive interactions, the proposed approach allows the robot to effectively navigate around obstacles, overcoming the classical limitations of APF associated with local minima. Experimental results confirm that the method enables precise engagement with the plant's cane while avoiding collisions between the blades and the plant, ensuring a safe and accurate pruning process.

ACKNOWLEDGMENT

This work has been performed under the project Vinum, a collaboration between IIT and the Department of Sustainable Crop Production at the Università Cattolica del ‘Sacro Cuore’, Prof. Matteo Gatti and Stefano Poni. This work is also part of the “Technologies for Sustainability” Flagship program of the IIT. Additional funding by the European Union -

NextGenerationEU and by the Ministry of University and Research (MUR), National Recovery and Resilience Plan (NRRP), Mission 4, Component 2, Investment 1.5, project “RAISE - Robotics and AI for Socio-economic Empowerment” (ECS00000035). Finally, the Vinum Project is partially funded and supported by RoboIT, the first National Technology Transfer Hub for Robotics and Industrial Automation, launched on the initiative of CDP Venture Capital SGR together with Pariter Partners and several players, including Istituto Italiano di Tecnologia.

REFERENCES

- [1] S. Poni, S. Tombesi, A. Palliotti, V. Ughini, and M. Gatti, “Mechanical winter pruning of grapevine: Physiological bases and applications,” *Scientia Horticulturae*, vol. 204, pp. 88–98, 2016.
- [2] M. Fernandes, A. Scaldaferrri, G. Fiameni, T. Teng, M. Gatti, S. Poni, C. Semini, D. Caldwell, and F. Chen, “Grapevine winter pruning automation: On potential pruning points detection through 2d plant modeling using grapevine segmentation,” in *IEEE Cyber*, 2021.
- [3] P. Guadagna, M. Fernandes, F. Chen, A. Santamaria, T. Teng, T. Frioni, D. Caldwell, S. Poni, C. Semini, and M. Gatti, “Using deep learning for pruning region detection and plant organ segmentation in dormant spur-pruned grapevines,” *Precision Agriculture*, vol. 24, pp. 1–23, 03 2023.
- [4] M. Fernandes, J. D. Gamba, F. Pelusi, A. Bratta, D. G. Caldwell, S. Poni, M. Gatti, and C. Semini, “Grapevine winter pruning: Merging 2d segmentation and 3d point clouds for pruning point generation,” *Computers and Electronics in Agriculture*, 2025.
- [5] B. Siciliano, L. Sciavicco, L. Villani, and G. Oriolo, *Robotics: modelling, planning and control*. Springer, 2009.
- [6] O. Khatib, “Real-time obstacle avoidance for manipulators and mobile robots,” in *Proceedings. 1985 IEEE international conference on robotics and automation*, vol. 2. IEEE, 1985, pp. 500–505.
- [7] J. Kuffner and S. LaValle, “Rrt-connect: An efficient approach to single-query path planning,” in *Proceedings 2000 ICRA. Millennium Conference. IEEE International Conference on Robotics and Automation. Symposia Proceedings (Cat. No.00CH37065)*, vol. 2, 2000, pp. 995–1001 vol.2.
- [8] M. Zhuang, G. Li, and K. Ding, “Obstacle avoidance path planning for apple picking robotic arm incorporating artificial potential field and a* algorithm,” *IEEE Access*, vol. 11, pp. 100 070–100 082, 2023.
- [9] X. Xia, T. Li, S. Sang, Y. Cheng, H. Ma, Q. Zhang, and K. Yang, “Path planning for obstacle avoidance of robot arm based on improved potential field method,” *Sensors*, vol. 23, no. 7, p. 3754, 2023.
- [10] C. De Medio and G. Oriolo, “Robot obstacle avoidance using vortex fields,” in *Advances in Robot Kinematics: With Emphasis on Symbolic Computation*. Springer, 1991, pp. 227–235.
- [11] A. Nasuha, A. Priambodo, and G. Pratama, “Vortex artificial potential field for mobile robot path planning,” in *Journal of Physics: Conference Series*, vol. 2406, no. 1. IOP Publishing, 2022, p. 012001.
- [12] A. S. Deo and I. D. Walker, “Overview of damped least-squares methods for inverse kinematics of robot manipulators,” *Journal of Intelligent and Robotic Systems*, vol. 14, no. 1, pp. 43–68, 1995.
- [13] R. . C. W. Group, “ros2_control documentation,” 2025. [Online]. Available: <https://control.ros.org/rolling/index.html>
- [14] D. Coleman, I. Sucan, S. Chitta, and N. Correll, “Reducing the barrier to entry of complex robotic software: a moveit! case study,” *Journal of Software Engineering for Robotics*, May 2014.